ChemPubSoc Europe

DOI: 10.1002/chem.201903178

CHEMISTRY A European Journal Full Paper

Metal–Organic Frameworks

Dynamic Interplay between Defective UiO-66 and Protic Solvents in Activated Processes

Chiara Caratelli,[a] Julianna Hajek,[a] Evert Jan Meijer,[b] Michel Waroquier,[a] and Veronique Van Speybroeck*[a]

Abstract: UiO-66, composed by Zr-oxide inorganic bricks $[Zr_6(\mu_3\text{-}O)_4(\mu_3\text{-}OH)_4]$ and organic terephthalate linkers, is one of the most studied metal–organic frameworks (MOFs) due to its exceptional thermal, chemical, and mechanical stability. Thanks to its high connectivity, the material can withstand structural deformations during activation processes such as linker exchange, dehydration, and defect formation. These processes do alter the zirconium coordination number in a dynamic way, creating open metal sites for catalysis and thus are able to tune the catalytic properties. In this work, it is shown, by means of first-principle molecular-dynamics simulations at operating conditions, how protic solvents may facilitate such changes in the metal coordination. Solvent can induce structural rearrangements in the material that can lead to undercoordinated but also overcoordinated metal sites. This is demonstrated by simulating activation processes along well-chosen collective variables. Such enhanced MD simulations are able to track the intrinsic dynamics of the framework at realistic conditions.

Introduction

Metal–organic frameworks (MOFs) are hybrid nanoporous materials that lie at the intersection between inorganic and organic chemistry. Their peculiar building concept, based on metal or metal-oxo clusters and organic linkers, allows for the creation of a plethora of structures with different topologies and functionalities. Moreover, these materials can further be tuned post synthetically through processes such as postsynthetic ligand exchange (PSLE),[1] in which linkers are functionalized to allow finetuning of the properties.[2] This tunability, along with their high metal content and porosity, makes them very appealing for many possible industrial applications,[3] ranging from catalysis[4] to gas storage and separation[5] or elimination of warfare agents.[6] The main drawback of this family of materials is their rather poor stability under reaction conditions. However, to date, a range of new chemically and thermally stable materials have been proposed, such as the Zr-MOF family.[7] Without any doubt, UiO-66[8] (displayed in Figure 1) composed by $[Zr_6(\mu_3\text{-}O)_4(\mu_3\text{-}OH)_4]$ bricks and terephthalate (BDC) linkers, is currently one of the most studied MOFs due to its exceptional stability,[9] that finds its origin in the high degree of connectivity of the framework. Each of the bricks in UiO-66 is connected to 12 ditopic BDC linkers and, within the brick, each of the six zirconium atoms is coordinated to four oxygen atoms belonging to the brick and four belonging to the linkers. In this perfect structure, zirconium atoms have a coordination number of 8. However, to activate these materials for catalysis, it is necessary to create open metal sites which can be realized by reducing the zirconium coordination. In this sense, structural defects may be incorporated in the material in the form of missing linkers or clusters,[10] without compromising the structural integrity. Such defects arise spontaneously during synthesis and their number can be tuned easily.[10a,c,11] Apart from these intentional defect creation, the material may also be thermally activated by dehydration at temperatures in the range of 250–330 °C.[12] Also in this case, the zirconium coordination number is reduced. Very recently, operando molecular dynamics (MD) simulations revealed that thermal activation of the brick leads to decoordination of the linkers. Such event can, in turn, push other linkers away from the brick triggering further decoordination in a cascade process in which new zirconium active sites are created.[13] It was postulated that these dangling linkers might possibly be stabilized by solvent interactions.

Recently, it has been shown that a protic solvent can play a crucial role in the stabilization of charged intermediates.[14] However, the exact role of a confined solvent in the pores of the material is so far unknown. Experimentally it was observed

[a] C. Caratelli, Dr. Ir. J. Hajek, Prof. Dr. M. Waroquier, Prof. Dr. Ir. V. Van Speybroeck
Center for Molecular Modeling, Ghent University
Technologiepark 46, 9052 Zwijnaarde (Belgium)
E-mail: Veronique.VanSpeybroeck@UGent.be

[b] Prof. Dr. E. J. Meijer
Van 't Hoff Institute for Molecular Sciences, University of Amsterdam
Science Park 904, 1098 XH Amsterdam (The Netherlands)

Supporting information and the ORCID identification number(s) for the author(s) of this article can be found under: https://doi.org/10.1002/chem.201903178.

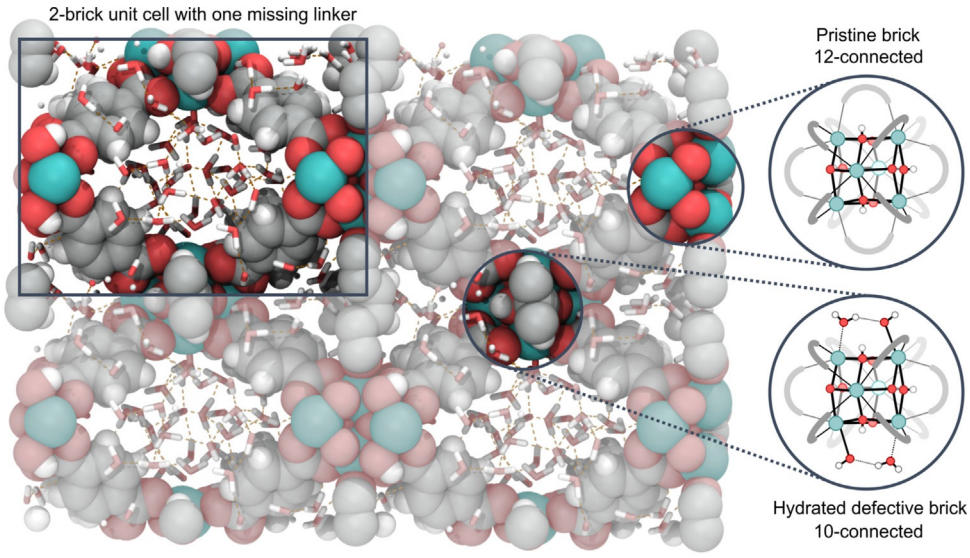

Figure 1. Representation of the defective 2-brick unit cell of UiO-66 used in the simulations, with solvent in the pores of the material. The unit cell is composed by one 12-connected pristine brick and one 10-connected hydrated defective brick, which are displayed on the right.

that methanol actively participates during the PSLE process. Even at low temperatures, UiO-66 is susceptible to ligand exchange with the aid of a solvent, without compromising the structural integrity of the material. It was postulated that intermediate metastable states are involved in the PSLE process, where linkers are dangling in the pores and remain only connected to one inorganic brick.[15] These rearrangements of the material point towards a dynamic interplay between the material and the confined protic solvent.[14] Dynamic coordination changes of zirconium are hard to track at the molecular level, therefore insight from simulations performed in this work can provide complementary understanding of how these processes take place.

Interestingly, in UiO-66 both hydrophilic and hydrophobic regions can be distinguished. It means that the interactions of a protic solvent confined in the pores of the material with the surface of the material may differ significantly and depend on the region in which the interaction is considered. When the interactions are strong, such as in the case of protic solvents interacting with hydrophilic regions of a material, new processes may be induced, which would not occur without the solvent or with aprotic solvent molecules. Within this respect, protic solvents will have strong interactions with the inorganic brick of UiO-66 and in particular with the defective sites. This was indeed confirmed by Ghosh et al.[16] who simulated adsorption isotherms for UiO-66 and indeed found that defects in the material play a crucial role in the adsorption properties, because these are the sites where water molecules are preferentially adsorbed. Yang et al. showed that the water topology of these defect sites can be tuned by methanol through the intermediacy of node methoxy groups.[17] So far, nanoscale insights into how the solvent may induce dynamic changes of the zirconium coordination number during activation processes are to a large extent missing. It poses a huge challenge to trace these intrinsic dynamics of the inorganic brick in situ experimentally. First-principle MD simulations at operating conditions, thus taking into account realistic temperatures and solvent loadings, have now become within reach.[18] Such approach is followed here and enabled us to reveal fundamentally new insights into the structural rearrangements of UiO-66.

With the aid of a protic solvent, zirconium sites can be undercoordinated and overcoordinated. Overcoordination of the zirconium atom by a water solvent can trigger a decoordination of the adjacent linkers and may thus be the onset for linker-exchange processes. Undercoordination, in contrast, is crucial for catalysis, where these defective sites serve as adsorption sites for reactive species and are responsible for the catalytic activity of the material.[19] Especially Lewis acid-catalyzed reactions profit from the accessibility of the metal site due to the defects generated by linker deficiencies. The catalytic activity of the material is clearly enhanced with the number and strength of the Lewis acid sites induced by the defects as demonstrated in earlier work of some of the authors of this manuscript with the citronellal cyclization as model reaction.[2b, 11] However, in some reactions performed in protic solvents conversion is also observed in the almost defect-free material, pointing towards a dynamic linker decoordination even at mild conditions,[20] which is also the necessary step for linker exchange.[15] The presence of protic solvents may furthermore induce a dual acid/base character of the catalyst by the appearance of Lewis and Brønsted sites. The latter sites inherently belonging to the Zr-oxide bricks can actively take part in the catalytic process, but their formation can even be enhanced by the presence of water molecules which can coordinate to the Zr-brick providing extra stabilization of various intermediates through hydrogen bonds,[14] as demonstrated in the study of the Fischer esterification of carboxylic acids with alcohols.[20b]

In this contribution, in situ molecular insight is obtained into the dynamic interactions between the defective UiO-66 material and a confined water and methanol loading, through usage of first principle MD simulations at operating conditions. We

show that the solvent is confined by hydrophobic interactions with the linkers but strongly interacts with the bricks and in particular with the defective sites. On the zirconium metal sites, water is strongly adsorbed and can be exchanged through a stepwise mechanism in which zirconium is undercoordinated or through a concerted one, which proceeds through an overcoordination of zirconium. Moreover, the overcoordination of the zirconium atom by solvent water can trigger a decoordination of the adjacent linkers. Our simulations follow the interplay between solvent and material and unravel for the first time the key process that leads to creation of diverse active sites, linker exchange, and defect formation at operating conditions.

Results and Discussion

To fully unravel the interaction between protic solvents and the defective UiO-66 material, three model systems have been constructed. The defective UiO-66 material is represented by a unit cell with two zirconium bricks and one missing linker, as schematically shown in Figure 1. In the simulations, a full loading of methanol and two different loadings of water are considered. For further details about the simulations, we refer to the computational methodology. A first step in the analysis consists in clearly identifying the type of interactions between the confined solvent and the material, which consists of both hydrophobic and hydrophilic regions. It is furthermore essential to identify the impact of the confinement on the structure of the solvent.[21] The changes resulting from the interaction between the host and the confined solvent, are monitored by investigating the vibrational density of states and radial-distribution functions (RDF) of the loaded framework, the empty framework, and bulk water. To this end, regular MD simulations are performed at working temperatures of 298 and 330 K.

At second instance, a series of enhanced sampling MD simulations are performed at operating conditions, to mimic activated processes which might be assisted or even induced by interactions with the protic solvents. Such processes rely on dynamic changes in the zirconium coordination number and may entail rearrangements of the inorganic brick, linker decoordination, or dynamic capping/decapping of defective sites with protic species. Such simulations may reveal molecular rearrangements which are hard to track from a purely experimental point of view. In the defective UiO-66 material two opposing factors contribute to the solvent–material interaction. On the one hand, the interaction between organic linkers and solvent is dominated by hydrophobic effects that confine the solvent in the pores. On the other hand, the $[Zr_6(\mu_3\text{-}O)_4(\mu_3\text{-}OH)_4]$ bricks offer hydrophilic Brønsted sites that interact through hydrogen bonding with the protic solvent and undercoordinated zirconium atoms that attract the solvent.

Interactions between protic solvents and hydrophobic and hydrophilic parts of the material

To understand the nature of the interactions between material and solvent, the vibrational density of states was generated by calculating the power spectra of the velocity autocorrelation functions of the atoms in the unit cell. By selecting specific atoms in the unit cell, it is possible to decompose the density of states into its different contributions. As such, two different spectra were generated for each simulation, separating the contribution of the material and the solvent (spectra in Figure 2, bottom). Moreover, to assign the peaks in the vibrational spectra to the corresponding molecular motions, the spectra were compared to the one obtained from total Hessian static calculations performed with the periodic VASP code[22] on the same unit cell without solvent and one hydroxyl group as charge-balancing species on each defect site (Figure S3, Supporting Information). By means of these static frequency calculations, it is possible to decompose the spectrum into the contributions of each single vibrational mode. This procedure gives insight into the changes which occur in the presence of a solvent.

The vibrational density of states obtained from the velocity autocorrelation function power spectrum of the framework atoms is shown in Figure 2 (bottom left). The results originate from MD simulations performed with the CP2K code[23] at the PBE-D3 level of theory on the framework with and without water and/or methanol. It is immediately clear that a distinction can be made between the frequency range below 1700 cm^{-1} and the range above 3000 cm^{-1}. The low-frequency spectrum is dominated by modes that involve deformations of the whole structure and motion of the linkers. This fingerprint region of the spectrum is characterized by vibrational modes that involve multiple parts of the system at the same time, therefore it is not always possible to assign peaks to isolated molecular motions. In this region, a small change in intensity between the empty (Figure 2, red curve) and solvated material (Figure 2, grey and blue curves) can be seen in the band at $\nu <$ 500 cm^{-1}. According to the static decomposition of vibrational modes, this is due to the slow rotation of the linkers along the axis that connects the two bricks and to deformations that change the pore shape and size. These modes are slightly affected by the interaction with the solvent molecules. Higher frequencies, up to 800 cm^{-1}, belong to distortions of the inorganic brick (collective motion of the Zr-atoms) and stretching of the Zr–O bonds with the μ_3-O and μ_3-OH groups. The peaks ranging from 800–1600 cm^{-1} are due to combinations of C–O, C–C stretching and bending and C–H bending vibrations of the linker atoms. For more details, a dual computational–experimental characterization of this frequency region in the case of the infrared spectrum has been reported by Valenzano et al.[9b] This part of the spectrum corresponds almost exactly to the empty material, in which no frequency shifts are observed when solvent is included, but only changes in intensity of the bands.

The high-frequency region above 3000 cm^{-1} is characterized by two sharp peaks related to C–H and O–H stretching. This part of the vibrational spectrum is clearly affected by the presence of a confined solvent (Figure 2 left, inset). The first peak is due to the stretching of the aromatic C–H bonds of the linkers. This peak in the presence of a solvent is slightly broadened but does not change in frequency. This weak broadening is

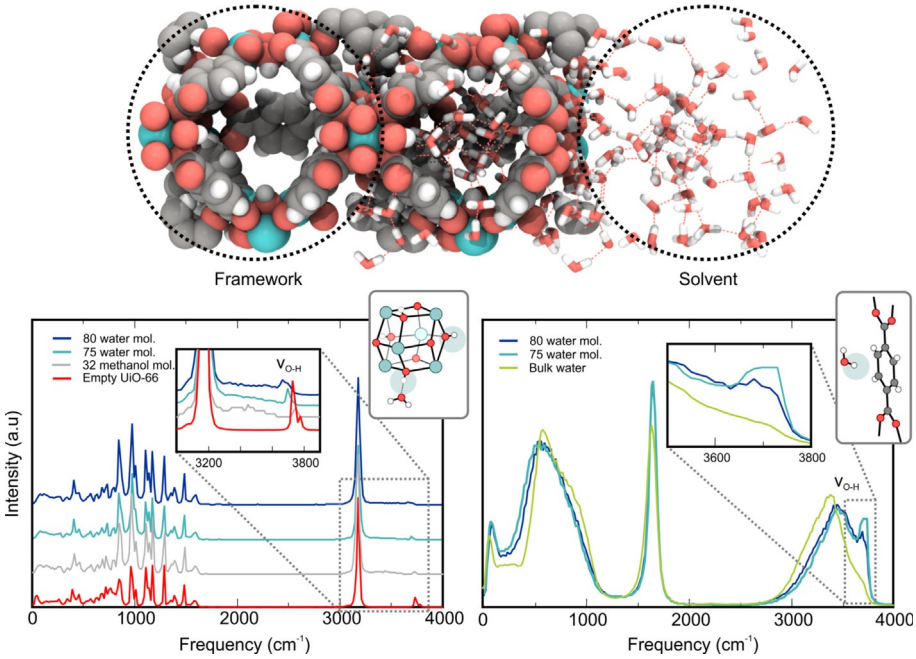

Figure 2. Top: schematic representation of the empty pore, pore with the solvent and confined solvent without the material. Bottom: vibrational density of states obtained from the velocity autocorrelation function power spectra of selected atoms of the simulation. Bottom left: solvated material compared with the empty material. Bottom right: water in the pores compared with bulk water.

most likely due to improper hydrogen-bond interactions[24] with the solvent. The most dramatic change in the spectrum can be seen in the peak at $\nu \approx 3750$ cm^{-1}. This peak arising in the spectrum of the empty material (Figure 2 left, red curve) is ascribed to the O–H stretching of the μ_3-OH groups of the brick and to the hydroxyl groups adsorbed on two of the defective zirconium atoms which serve as charge-balancing species. Upon introduction of a solvent, we observe a shift of this peak to lower frequencies, as well as a strong broadening. This is due to strong hydrogen-bond interactions with the solvent. Previous results indicate that the lower vibrational spectrum related to the structural part of the material is barely influenced by the presence of water, whereas the higher vibrational part related to O–H vibrational modes of the inorganic brick are very sensitive to the presence of protic solvents.

To specifically understand the impact of the material on the solvent properties, we compared the vibrational density of states of the confined solvent (Figure 2 right, blue curves), with the vibrational density of states for bulk water whereby the simulation has been performed in the same unit cell at the same conditions (Figure 2 right, green curve). The modes below 1000 cm^{-1} associated to librations and diffusion seem to be slightly shifted towards lower frequencies in case of confinement, indicating that the water molecules are submitted to slower rearrangements due to a tighter network of hydrogen bonds in case of a confined solvent.[25] No changes are noticed in the sharp bending peak at 1700 cm^{-1}. The most striking feature in these spectra is the appearance in the confined liquid of a peak at $\nu > 3700$ cm^{-1}, which is due to O–H bonds which are not hydrogen bonded, in line with what is observed in case of a hydrophobic confinement.[21,26] These should be identified as O–H bonds of water molecules pointing towards the hydrophobic linkers.

The hydrophobic and hydrophilic parts of the material can also be delimited from radial distribution functions (RDFs) which offer a measure on how the density of the particles varies as a function of the distance from another tagged particle and form important structural characteristics. In our study, we calculate RDFs for pairs of atoms belonging to the material and the solvent in a unit cell with a loading of 80 water molecules. These RDFs are reported in Figure 3, along with their integrated values, which show the number of correlated pairs that give rise to each RDF peak. We refer to the Supporting Information for a more detailed discussion.

RDFs between the linker atoms and the water atoms (shown in the upper panel of Figure 3) show a typical behavior for a hydrophobic confinement and are similar to what has been observed in carbon nanotubes.[26b] The RDF corresponding with the C(l)–O(w) pair (black curve) is nearly zero for distances below 3 Å after which it increases sharply, whereas the C(l)–H(w) RDF (light-grey curve) starts at lower values. This is an indication that the hydrogens of the water molecules near the interface have a slight preference to orient themselves towards the aromatic carbons. In contrast, the RDFs between water and oxygens of the brick and linkers in the middle panel of Figure 3 are more structured due to stronger interactions between material and solvent. In particular, the water molecules interact strongly with the oxygens of the inorganic brick (μ_3-OH, dark-red curve and μ_3-O, red curve). The correlation between a μ_3-OH oxygen atom and an adjacent water molecule is stronger than with a μ_3-O, in agreement with the weak acidity of the μ_3-OH hydrogen reported for some reactions.[20b,27]

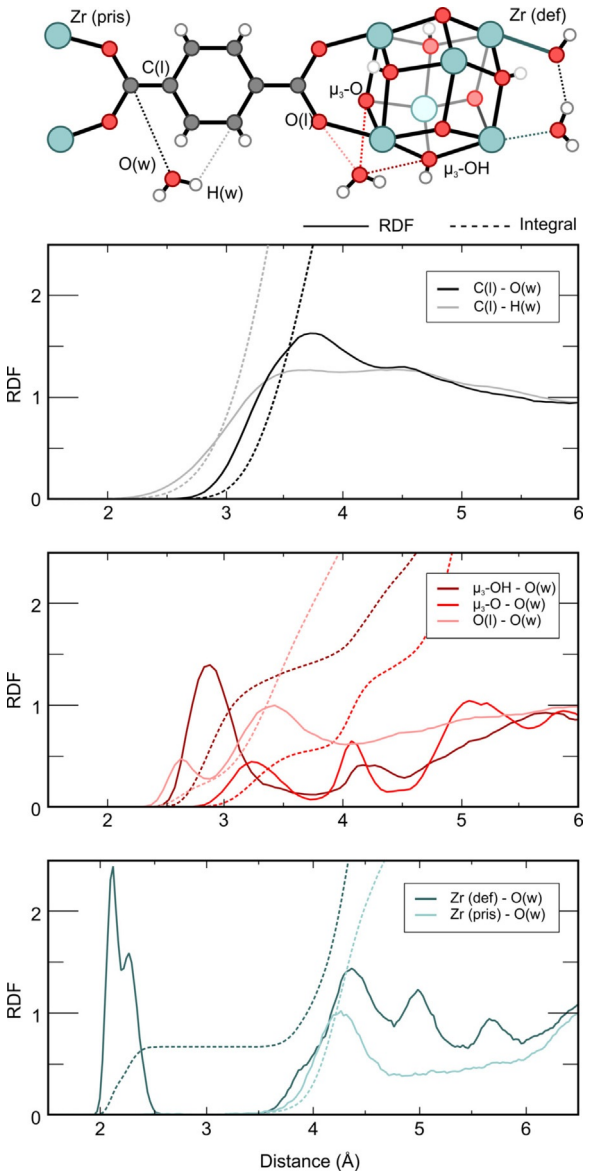

Figure 3. Radial distribution functions between oxygen and hydrogen of water (O(w), H(w)) and different atoms of the material obtained from the simulation with 80 water molecules in the unit cell. Full lines indicate the RDF, dashed lines indicate its integral. Upper panel: RDFs between water and linker carbons C(l); middle panel: RDFs between water and oxygen atoms of the linkers and bricks (O(l), μ_3-OH, μ_3-O); lower panel: RDFs between water and zirconium atoms of defective and pristine bricks (Zr(def), Zr(pris)).

The RDF between the carboxylic oxygens of the linkers (pink curve) and the oxygens of the water molecules also shows a stronger interaction at shorter distances than the C(l)–O(w) RDF and formation of a network of hydrogen bonds with the water molecules. Finally, we investigate the coordination between the Zr-atoms of the brick and the water molecules. In the case of a defective brick the first peak at 2.1–2.3 Å is due to the adsorption of water or hydroxy species on the undercoordinated Zr-atom at the defect site. At the pristine brick the RDF starts at much larger distances, because water molecules are rather coordinated to other parts of the brick such as the μ_3-OH oxygen atoms.

Summarizing, the various RDFs give valuable structural information on the confinement effect of water solvent in the pores of a defective UiO-66 material and the partition of hydrophilic and hydrophobic regions. However, the reported RDFs are average distributions measured over the whole simulation time and do not give a reflection of the dynamic processes which occur during the simulations. Processes such as dynamic proton acidity, decoordination of water from the active sites or linker decoordination can lead to dynamic fluctuation of the coordination environment of the zirconium atoms. This can have a drastic effect on the nature, type, and number of active sites, which in turn substantially affects the catalytic properties of the material. These fluctuations will be examined in detail in the next section.

Activated processes related to dynamic changes in the zirconium coordination number

Herein, we focus on the dynamic changes of the zirconium coordination numbers of the hydrated defective brick as displayed in Figure 1. In its hydrated form, each zirconium atom on the defect site has a total coordination number of eight. Previous regular MD simulations do not show any changes in the coordination numbers, neither in water nor in methanol solvent. The energetically favorable substitution of defect coordinating water by methanol postulated in previous works[15,17,20b] was not observed. However, RDFs (Figure 3) point towards some large fluctuations of the zirconium–water coordination bonds. Breaking of zirconium–oxygen coordination bonds typically occurs during activation processes, such as dehydration, defect formation and PSLE. To simulate the behavior of the material under these conditions, we need to apply enhanced sampling MD simulations which allow to steer the system towards higher lying regions of the free-energy surface.[28] In this case we performed a series of independent metadynamics simulations, which enabled to enhance the sampling of some low-probability regions along certain coordinates of the system, denoted as collective variables (CVs) which describe the coordination state of zirconium. We particularly focus on water as protic solvent in these simulations, because it possesses a higher number of mobile protons than methanol, thus better stabilizing intermediate configurations. Moreover, we can better follow the dynamics of the system because the defect-coordinating water species are the same as the rest of the solvent.

A first CV, displayed in Figure 4a, represents the coordination CN_W between a zirconium atom on the defect site and the oxygen atoms of the surrounding water molecules. In the formula, r_i is the zirconium–oxygen distance, whereas r_0 represents a cutoff distance of 2.9 Å, representative for a physisorbed water at the zirconium atom. This value may be derived readily from the RDF of Figure 3. Only the oxygen atoms that are inside this coordination sphere (represented in green) contribute to the coordination with the metal. To better monitor the variations, the coordination number is taken as relative with respect to the equilibrium value ($CN_{W,eq} = 1$). For example, at equilibrium conditions, where the zirconium atom is eight-

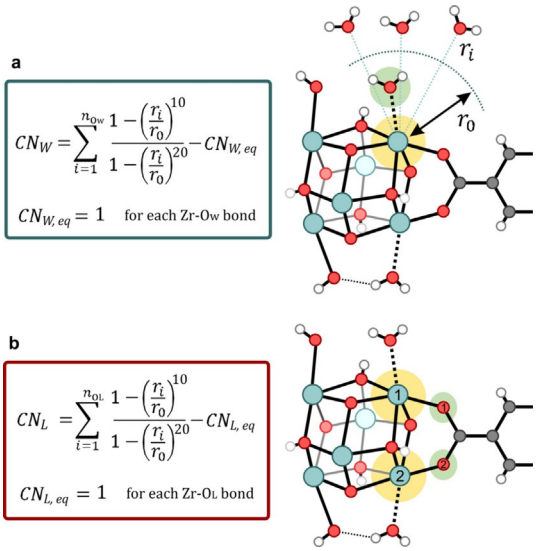

Figure 4. Coordination numbers used in the simulation a: coordination number CN_W between zirconium and all water oxygens. Also, the linker that induces changes in the zirconium coordination number is visualized. b: coordination number CN_L between each zirconium atom and linker oxygen atoms. n_{OW} and n_{OL} are the number of oxygen atoms considered in the two cases, r_i is the zirconium-oxygen distance, r_0 a cutoff distance of 2.9 Å. In yellow, the zirconium atoms considered in the *CN*. In green, the oxygen atoms that have a weight close to one and substantially different from zero in the summation.

fold coordinated, $CN_W = 0$, whereas $CN_W = -1$ when water decoordinates from the active site. The second relevant CV is the coordination number CN_L that describes the coordination of the defect-bridging linker to the zirconium atoms of the brick. It is defined in a similar way, but with the coordination bond length r_i equal to the zirconium–carboxylate oxygen distance (Figure 4b). In this case, we also consider the CN as relative to the equilibrium value (for each Zr–O_L bond, $CN_{L,eq} = 1$). A value $CN_L = 0$ means that the linker is in the equilibrium configuration and is entirely coordinated to the two zirconium atoms of the brick as displayed in Figure 4b. If one of the bonds is broken, then $CN_L = -1$.

Various MTD simulations were performed which reveal how the system behaves when the zirconium coordination number changes upon enhanced sampling along one of these two collective variables. Using the coordination numbers CN_W and CN_L it is possible to describe many events that occur around the brick and which are reported schematically in Figure 5. In the equilibrated structure at operating conditions, each zirconium atom belonging to the defective brick is eightfold coordinated and we can define this state as (0,0), where the first number refers to CN_W and the second to CN_L. The coordination changes of the zirconium atoms can be easily deduced by the values of the two collective variables: if $CN_L + CN_W < 0$, such as in the states (−1,0) or (0,−1) there is an undercoordination, whereas $CN_L + CN_W > 0$, such as in (+1,0), means overcoordination.

Undercoordinated zirconium states have already been reported in literature, for example in the work of Hajek et al.[13,20b] However, overcoordinated states have not been explicitly reported so far. Various possibilities for the rearrangements around the inorganic brick are shown in Figure 5. When inspecting the starting structure of the inorganic brick, the easiest way to induce undercoordination and creation of Lewis acid sites is the decoordination of one physisorbed water (state (−1,0) in Figure 5). Another possibility is the breakage of a zirconium–oxygen bond with one of the organic linkers (state (0,−1) in Figure 5). Overcoordination might in principle occur when more water molecules are coordinated to the zirconium atoms (state (1,0) in Figure 5). These are all events which may take place, however at this moment it is still unclear whether such processes actually occur during activation and what the effect of such events would be on the other coordination bonds of the inorganic brick, as well as how the solvent around the inorganic brick would respond to such rearrangements. Possible events are schematically shown in Figure 5. To estimate the occurrence of these events, a series of independent metadynamics simulations are performed as sketched below.

In a first case study, we consider the coordination number CN_W between one of the zirconium atoms of the defective site and water oxygens as CV, as already proposed by Lau and Ensing.[29] In principle CN_W, as defined in Figure 4, includes contributions of all solvent water molecules of the unit cell. In a dynamic process, water molecules can migrate in or outside the coordination sphere. The MTD calculation was started from

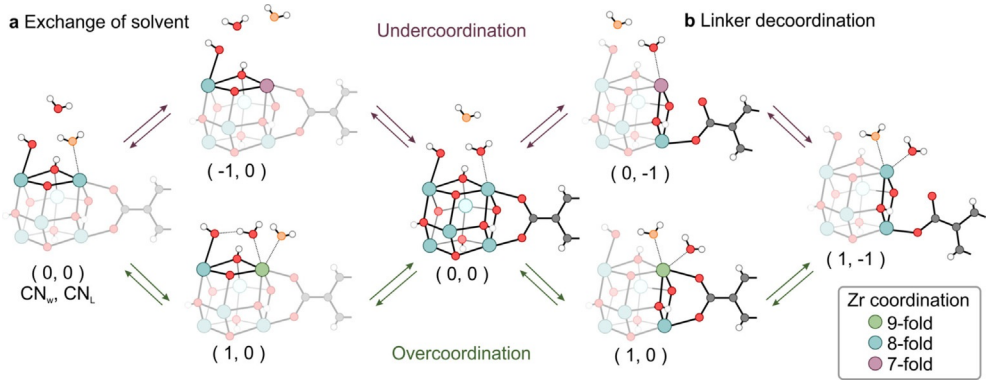

Figure 5. Coordination and value of the CVs during (a) the exchange of solvent and (b) linker decoordination in the MTD simulations. top paths: stepwise pathway which goes through undercoordinated zirconium; bottom paths: concerted pathways which go through overcoordinated zirconium.

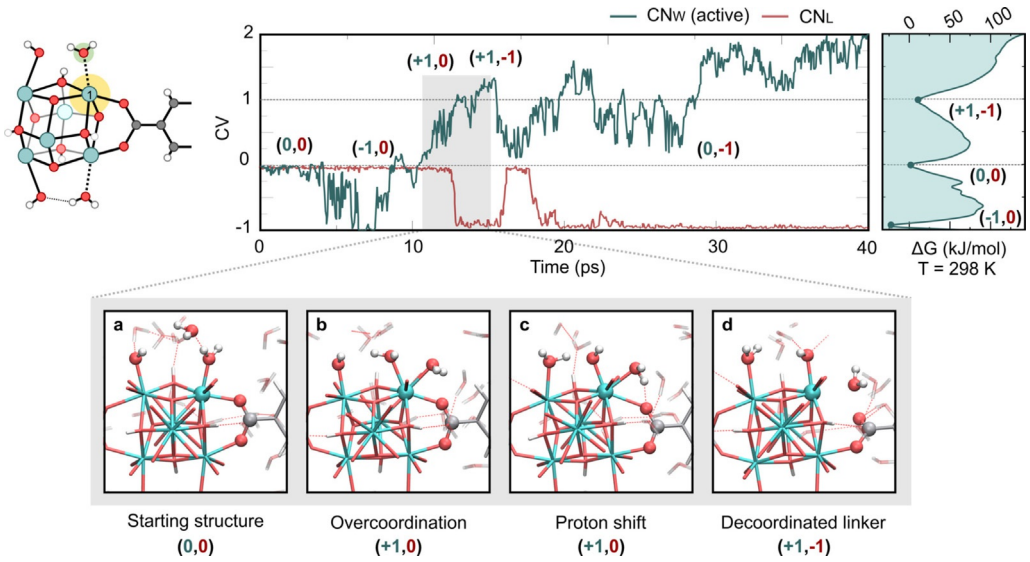

Figure 6. Top: time evolution of the collective variable and free-energy profile for the first MTD simulation along the CV representing the coordination CN_W between the zirconium atom Zr1, highlighted in yellow and all water molecules (green curve). CN_L between Zr1 and the neighboring defect-bridging linker oxygen (red curve) is also monitored; bottom: snapshots on the linker decoordination triggered by overcoordination.

an equilibrated structure obtained from the previous MD simulation with 80 water molecules in the unit cell. The time evolution of the collective variable is plotted in Figure 6, where 0 is taken as the reference where the zirconium atom is eightfold coordinated. Negative values for the CV correspond to undercoordination of the zirconium atom, whereas positive values indicate an overcoordination. At the same time, the coordination with the linker that induces changes in the total coordination of the same zirconium atom (Zr1, highlighted in yellow) is also monitored. In the beginning of the simulation at equilibrium, the coordination number between the zirconium atom and this linker is 1, therefore $CN_L = 0$. In this sense, we start from an equilibrium configuration which is labelled (0,0), referring to $CN_W = 0$ and $CN_L = 0$. After 4 ps, the water molecule coordinated to the zirconium atom leaves the coordination sphere, creating a temporarily undercoordinated zirconium site (configuration (−1,0)). The large fluctuations of the CV between −1 and 0 after 4 ps suggest that water is dynamically re-entering the coordination sphere. The decoordination leads to the formation of a Lewis acid site in which reactants can adsorb and which may represent the active site in catalytic processes. The system dynamically explores configurations in which the zirconium atom is temporarily undercoordinated and in which another water molecule can then re-enter the coordination sphere. In this undercoordinated pathway, the dynamic exchange of a solvent molecule occurs after the metal site has been opened (Figure 5a), with a free-energy barrier in the order of 70 kJ mol^{-1}.

Given that the exact free energies may be quite dependent on various computational degrees of freedom, such as choice of the CV and level of theory, the values given here should be interpreted as a qualitative measure rather than an exact quantitative estimate of the barrier. More details about the free energy profiles and the regions visited by the two collective variables are provided in the Supporting Information.

When further proceeding the MTD simulation, the system explores configurations in which the zirconium atom is overcoordinated going to a ninefold coordination. It is interesting to mechanistically follow the rearrangements of the solvent around the inorganic brick. After about 11 ps we observe a series of states which are pictorially represented in Figure 6a–d, bottom panel. First, a water molecule coming from the pore inserts between the Zr–H_2O and the Zr–OH groups (Figure 6a) and pushes the physisorbed molecule towards the side of the pore. This third water molecule is now very close to the Zr–OH group (Figure 6b) and forms a strong hydrogen bond with it, leading to a proton shift. The zirconium atom is now coordinated to a hydroxyl group and to a water molecule. The Zr–OH bond on the ninefold coordinated zirconium is thus stronger and pushes the water molecule even more strongly to the side (Figure 6c). Simultaneously, the water molecule that was pushed away forms a hydrogen bond with the linker, which is in turn decoordinated from the zirconium atom, bringing the zirconium atom back to the more stable eightfold coordination. This results in configuration (+1,−1) with a partially decoordinated linker (Figure 6d), which is stabilized by hydrogen bonds with the solvent. The free-energy barrier needed to come into this overcoordinated state amounts to about 60 kJ mol^{-1} and is of the same order of magnitude needed to visit the undercoordinated state. A barrier of the same order was reported by Zahn et al.[30] for the nucleation and growth of the Zr–fumarate MOF, isoreticular to UiO-66. Such barrier refers to the mechanism of substitution of a modulator molecule by a linker on the zirconium atom. After this event, the linker sometimes temporarily recoordinates to the zirconium but decoordinates shortly again hereafter. From now on the system remains in a regime with CVs fluctuating between 0 and 2 and the zirconium atom coordination ranging from 7 to 9. The states encountered here, with partially decoordinated linkers might be important configurations for PSLE. Previous

simulations clearly show the crucial role of solvent water, inducing the coordination changes of zirconium and helping to stabilize the partially disconnected linkers. During this biased simulation we observed a dynamic evolution of the system and a creation of a plethora of active sites that are generated through different mechanisms.

Similar as in the first study case, we also performed a MTD simulation starting from an initial structure with focus on the coordination of the water molecules with a zirconium atom on the other side of the defective brick. The processes encountered during this simulation are similar compared to previous case, with solvent exchange by undercoordination and overcoordination of the zirconium atoms, as well as linker decoordination. To account for possible proton transfers, a similar MTD simulation was performed involving both adjacent zirconium atoms instead of a single zirconium site. The encountered processes are similar, but we see that also the Zr–OH group can be decoordinated to allow the creation of two adjacent Lewis sites. The OH^- species is stabilized by the solvent and can be further protonated by other solvent molecules. More detailed results are reported in the Supporting Information (Figures S9–S18).

In the second case study we investigate the decoordination of one linker by performing a MTD simulation along the linker coordination number CN_L as collective variable, as visualized in the initial structure of Figure 7. In this case, we are directly enhancing the sampling along states where the coordination of two zirconium atoms with the organic linker may vary. The evolution of the collective variable is displayed in Figure 7.

The simulation starts in the equilibrium structure where each zirconium atom is eightfold coordinated, as shown in Figure 7a (configuration (0,0)). At the same time, we are monitoring the coordination of the two active zirconium atoms (Zr1 and Zr2, highlighted in yellow) with all water molecules. This coordination is indicated as CN_W in the Figure and its value is relative to its equilibrium value $CN_{W,eq}=2$ ($CN_{W,eq}=1$ for each zirconium atom, as shown in Figure 5). After some picoseconds, the system explores regions in which one bond of the linker is broken due to a rotation of the linker (Figure 7b, configuration (0,−1)). The free energy associated to this decoordination is of the order of 50 kJ mol^{-1}. Translation of the linker is also observed, which results in a metastable chelated structure displayed in Figure 7c, in which both oxygens are coordinated to the same zirconium atom. After about 28 ps of simulation, states are explored in which the second bond is also broken leading to a dangling-linker state (Figure 7d, configuration (0,−2)). This state is associated to a higher energy barrier than the first Zr–O bond cleavage. However, this barrier is overestimated due to the short simulation time compared with the longer time scale of the event, which should involve diffusion and adsorption of solvent. As reported by Paesani et al., the diffusion constant of water in the pores is decreased by one order of magnitude for MIL-53 compared with the bulk.[25b] This type of simulation demonstrates a pathway for the breakage of the zirconium–oxygen bond with the linker, without overcoordination of the zirconium atom by the solvent. The role of the solvent, however, is expected to be important, because it plays a role in stabilizing the dangling linker through hydrogen bonding with the carboxylic oxygen. The simulation does not display minima on the free energy profile, at $CV=-1$ and $CV=-2$ because in these states the zirconium atom remains undercoordinated. One can imagine that if a water molecule diffuses from the pore and coordinates to the undercoordinated zirconium atom, this would restore the eightfold coordination, lowering the energy. However, during the simulation time, this event is not observed. The interactions around the linkers are dominated by hydrophobic effects and the solvent molecules are hindered by the dynamic motions of the linker.

Summarizing, based on different biased simulations, we come to the conclusion that some features like the solvent exchange and linker decoordination may result from either an undercoordinated or overcoordinated configuration of the zir-

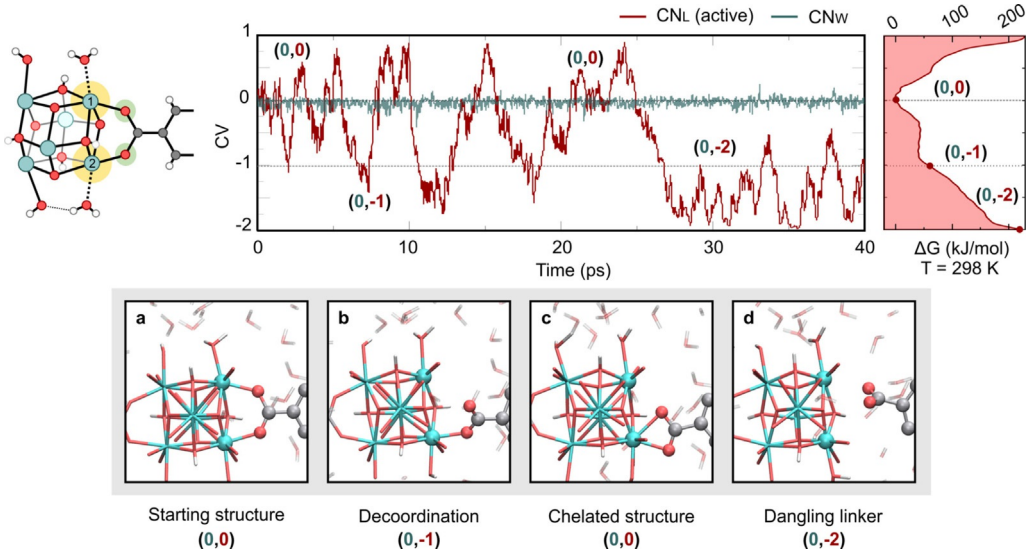

Figure 7. Top: time evolution of the collective variable and free energy profile for the second MTD simulation along the CV representing the coordination CN_L between the zirconium atoms Zr1 and Zr2, highlighted in yellow and the two linker atoms highlighted in green (red curve). CN_W between Zr1 and Zr2 and the solvent oxygens (green curve) is also monitored; bottom: snapshots on the linker decoordination.

conium atom. Solvent exchange (Figure 5a) can proceed through a stepwise mechanism, characterized by a temporary undercoordination of the zirconium atoms or a concerted mechanism, in which the zirconium atom is temporarily overcoordinated. A similar pattern is observed for the linker decoordination (Figure 5b). The metal–linker bond can be broken directly, without influence of the solvent, leading to an undercoordination of the zirconium atom, but can also be broken as a result of an overcoordination of an additional solvent molecule. Moreover, solvent can stabilize the intermediate configurations along the process and assist in stabilizing the charged species through hydrogen bonding.

In earlier work we had already observed mobility of the linkers in the brick at activation conditions,[13] but this is the first time that such process has been computationally modelled at catalytic conditions in the presence of a solvent and this mobility does not involve any rearrangement of the brick. The dangling linkers shown in these simulations are perfectly in line with the experimentally reported decrease in BET surface area during the PSLE process caused by a hindrance of the pores. Such exchange is reported already at low temperature of 313 K and all experimental evidence points towards the creation of dangling linkers states by modulation of the zirconium coordination by the protic solvent.[15] Moreover, the group of Cohen showed that the exchange rate is strongly correlated to the polarity of the solvent in which the process takes place.[31] The proposed mechanisms support the lower resistance of UiO-66 series to bases compared with acids reported by Kandiah et al.,[1b] because bases present in solution can more easily compete with linkers and break the Zr–O bonds. Also the growth of MOF structures in presence of modulator can proceed through similar process, governed by a modulation of the zirconium coordination.[30] These findings are in line with the possible hydrolysis of the metal–ligand bond in MOFs in the presence of water that was proposed in a previous theoretical work[32] and with the lability of the organic SBUs in presence of a solvent.[33] Other MOFs can be hydrolyzed through such mechanisms, whereas UiO-66 remains very stable in the presence of water[34] due to its high structural connectivity. Nevertheless, the reported first principle MD simulations at operating conditions show how the UiO-66 material can be structurally modified. The temporary decoordination of linkers proposed here can explain the relatively high conversion of the defect-free UiO-66 material for certain dual Lewis/Brønsted catalyzed reactions. For instance, for the final product of the Oppenauer oxidation it was possible to obtain a conversion of more than 60% on the almost defect-free UiO-66 material (11.6 linkers / brick).[20a] A conversion of more than 40% is obtained after 8 hours for Fischer esterification (11.8 linkers / brick) although the process is slower than in the more defective material.[20b]

Conclusions

This work examines the structural integrity of defective UiO-66 material and the role of a protic solvent as water and methanol in sustaining structural rearrangements in the material at operating conditions. Earlier work gave evidence for the exceptional stability of the empty UiO-66 even during processes in which linkers become mobile. Such events were observed during simulations of the dehydration process of the material. On the one hand we observed that the structure of the solvent is impacted by both its hydrophobic and hydrophilic interactions with the framework. However, the structure of the material remains intact in the presence of protic solvents. On the other hand, we simulated some activated processes which may lead to coordination changes of the zirconium atom. The strong tendency of the solvent molecules to adsorb on the zirconium atom and the possible hydrogen-bond stabilization with linkers, allow a dynamic behavior of the linkers. These findings shed light on the exceptional dynamic stability of the defective UiO-66 material and its dynamic interactions with protic solvents during post synthetic treatment. These interactions may indicate a dynamic response of the material during catalytic processes in some protic solvents, in which linkers may temporarily decoordinate creating Lewis acid sites. The observed fluctuating coordination number of the zirconium atoms at the defect site gives a variable Lewis acidity to the metal, offering ideal opportunities to induce Lewis catalyzed reactions. Finally, we have observed for the first time how overcoordination of the zirconium atom with solvent water can tune the structural properties of the material. This can be the first step in activation processes such as PSLE, but also in other processes in which active sites are generated. The exceptionally high connectivity of the material allows for a whole plethora of dynamic events in which linkers, bricks and solvent can exchange without altering the stability of the structure.

Computational Methodology

The investigated structures were constructed from an optimized 2-brick unit cell where one linker has been removed, selected among the possible structures proposed in the work of Rogge et al. and De Vos et al.[35] Starting structures in which the solvent is introduced in the pores are generated with Monte Carlo simulations (MC). Regular MD calculations on the empty and solvated unit cells and bulk solvent were performed to gain insight at equilibrium conditions, followed by MTD simulations.

In the static and dynamic ab initio calculations we made use of PBE-D3 functional given the good balance between accuracy and computational cost. PBE together with dispersion interactions has been shown to give good results for modeling structures of nanoporous rigid and flexible MOFs.[36] This functional has been extensively used in previous static and dynamic studies.[37] Although known to overestimate the strength of hydrogen bonds,[38] PBE represents the obvious choice to capture the dynamic processes on the defective sites shown in this work. More details on the choice of the functional are reported in the Supporting Information (Table S1).

Starting structures calculations

The static calculations on the UiO-66 unit cell were performed with a periodic density functional theory (DFT) approach. The methodology and level of theory used were the same as in previous works of the presenting authors.[14] The periodic VASP code[22] was used

applying the projector augmented wave approximation (PAW)[39] with gamma point approximation. We optimized the empty UiO-66 unit cell at the PBE-D3 level of theory.[40] The energy cutoff was set to 700 eV, with a 10^{-5} eV convergence threshold for the electronic SCF calculations and a gaussian smearing of 0.025 eV was included. Total Hessian frequency calculations were performed for this structure using finite displacements. To generate starting structures, MC calculations have been performed using the RASPA software.[41] Two solvated structures were generated with 80 and 75 water molecules adsorbed in the unit cell. The value of 80 water molecules corresponds to what is reported by Ghosh et al.[16] in the same defective UiO-66 unit cell at 1 bar and 298 K, obtained by Grand Canonical MC simulations performed with RASPA. MC simulations were also used to generate the bulk solvent unit cells, in which the number of molecules was chosen to replicate the experimental density.

MD simulations

The DFT MD simulations were performed using the CP2K simulation software[23] with the PLUMED code.[42] The electronic structure was determined with the PBE-D3 functional,[40] employing a DZVP-MOLOPT-GTH basis set and GTH pseudopotentials.[43] A hybrid Gaussian–plane wave basis set approach[44] was used, with a cutoff of 400 Ry. The level of theory was chosen for better comparison with previous static and dynamic results. The time step was set to 0.5 fs and a Nosé-Hoover thermostat with five beads and 0.3 ps time constant was used to set the temperature to 298 K for water and 330 K for methanol.[45] The unit-cell volume was equilibrated in the NPT ensemble at the simulation temperature and 1 bar using a MTK barostat with 0.1 ps time constant.[46] Given the rigidity of the material, the average volume was used in the following simulations performed in the NVT ensemble.

Metadynamics simulations

To sample the activated states, metadynamics simulations have been performed[28a,b] starting from the equilibrated NVT simulations. Gaussian hills are added every 25 fs along a chosen CV, which represents the coordination between zirconium and water molecules or zirconium and carboxylate oxygens of a linker. A 1D free-energy diagram can be reconstructed from this bias potential. More details are reported in the Supporting Information (Figure S9–S18).

Acknowledgements

This project has received funding from the European Union's Horizon 2020 research and innovation program under the Marie Skłodowska-Curie (grant agreement No 641887, acronym: DEFNET). The authors further acknowledge financial support from the European Research Council (consolidator ERC Grant Agreement No 647755—DYNPOR (2015–2020)) and the Research Board of Ghent University (BOF). The computational resources and services used in this work were provided by the VSC (Flemish Supercomputer Center), funded by the Hercules foundation and the Flemish Government—department EWI.

Conflict of interest

The authors declare no conflict of interest.

Keywords: density functional calculations · metal–organic frameworks · molecular dynamics · solvent · UiO-66

[1] a) S. J. Garibay, S. M. Cohen, *Chem. Commun.* **2010**, *46*, 7700 – 7702; b) M. Kandiah, M. H. Nilsen, S. Usseglio, S. Jakobsen, U. Olsbye, M. Tilset, C. Larabi, E. A. Quadrelli, F. Bonino, K. P. Lillerud, *Chem. Mater.* **2010**, *22*, 6632 – 6640; c) M. Kim, J. F. Cahill, H. Fei, K. A. Prather, S. M. Cohen, *J. Am. Chem. Soc.* **2012**, *134*, 18082 – 18088.

[2] a) F. Vermoortele, R. Ameloot, A. Vimont, C. Serre, D. De Vos, *Chem. Commun.* **2011**, *47*, 1521 – 1523; b) F. Vermoortele, M. Vandichel, B. Van de Voorde, R. Ameloot, M. Waroquier, V. Van Speybroeck, D. E. De Vos, *Angew. Chem. Int. Ed.* **2012**, *51*, 4887 – 4890; *Angew. Chem.* **2012**, *124*, 4971 – 4974.

[3] H. Furukawa, K. E. Cordova, M. O'Keeffe, O. M. Yaghi, *Science* **2013**, *341*, 1230444.

[4] J. Liu, L. Chen, H. Cui, J. Zhang, L. Zhang, C.-Y. Su, *Chem. Soc. Rev.* **2014**, *43*, 6011 – 6061.

[5] J.-R. Li, R. J. Kuppler, H.-C. Zhou, *Chem. Soc. Rev.* **2009**, *38*, 1477 – 1504.

[6] a) J. E. Mondloch, M. J. Katz, W. C. Isley III, P. Ghosh, P. Liao, W. Bury, G. W. Wagner, M. G. Hall, J. B. DeCoste, G. W. Peterson, R. Q. Snurr, C. J. Cramer, J. T. Hupp, O. K. Farha, *Nat. Mater.* **2015**, *14*, 512 – 516; b) A. M. Plonka, Q. Wang, W. O. Gordon, A. Balboa, D. Troya, W. Guo, C. H. Sharp, S. D. Senanayake, J. R. Morris, C. L. Hill, A. I. Frenkel, *J. Am. Chem. Soc.* **2017**, *139*, 599 – 602.

[7] Y. Bai, Y. Dou, L.-H. Xie, W. Rutledge, J.-R. Li, H.-C. Zhou, *Chem. Soc. Rev.* **2016**, *45*, 2327 – 2367.

[8] J. H. Cavka, S. Jakobsen, U. Olsbye, N. Guillou, C. Lamberti, S. Bordiga, K. P. Lillerud, *J. Am. Chem. Soc.* **2008**, *130*, 13850 – 13851.

[9] a) K. Leus, T. Bogaerts, J. De Decker, H. Depauw, K. Hendrickx, H. Vrielinck, V. Van Speybroeck, P. Van Der Voort, *Microporous Mesoporous Mater.* **2016**, *226*, 110 – 116; b) L. Valenzano, B. Civalleri, S. Chavan, S. Bordiga, M. H. Nilsen, S. Jakobsen, K. P. Lillerud, C. Lamberti, *Chem. Mater.* **2011**, *23*, 1700 – 1718.

[10] a) O. V. Gutov, M. G. Hevia, E. C. Escudero-Adán, A. Shafir, *Inorg. Chem.* **2015**, *54*, 8396 – 8400; b) G. C. Shearer, S. Chavan, J. Ethiraj, J. G. Vitillo, S. Svelle, U. Olsbye, C. Lamberti, S. Bordiga, K. P. Lillerud, *Chem. Mater.* **2014**, *26*, 4068 – 4071; c) G. C. Shearer, S. Chavan, S. Bordiga, S. Svelle, U. Olsbye, K. P. Lillerud, *Chem. Mater.* **2016**, *28*, 3749 – 3761; d) M. J. Cliffe, W. Wan, X. Zou, P. A. Chater, A. K. Kleppe, M. G. Tucker, H. Wilhelm, N. P. Funnell, F.-X. Coudert, A. L. Goodwin, *Nat. Commun.* **2014**, *5*, 4176.

[11] F. Vermoortele, B. Bueken, G. L. Le Bars, B. Van de Voorde, M. Vandichel, K. Houthoofd, A. Vimont, M. Daturi, M. Waroquier, V. Van Speybroeck, *J. Am. Chem. Soc.* **2013**, *135*, 11465 – 11468.

[12] G. C. Shearer, S. Forselv, S. Chavan, S. Bordiga, K. Mathisen, M. Bjorgen, S. Svelle, K. P. Lillerud, *Top Catal.* **2013**, *56*, 770 – 782.

[13] J. Hajek, C. Caratelli, R. Demuynck, K. De Wispelaere, L. Vanduyfhuys, M. Waroquier, V. Van Speybroeck, *Chem. Sci.* **2018**, *9*, 2723 – 2732.

[14] C. Caratelli, J. Hajek, S. M. J. Rogge, S. Vandenbrande, E. J. Meijer, M. Waroquier, V. Van Speybroeck, *ChemPhysChem* **2018**, *19*, 420 – 429.

[15] J. Marreiros, C. Caratelli, J. Hajek, A. Krajnc, G. Fleury, B. Bueken, D. E. De Vos, G. Mali, M. B. J. Roeffaers, V. Van Speybroeck, R. Ameloot, *Chem. Mater.* **2019**, *31*, 1359 – 1369.

[16] P. Ghosh, Y. J. Colon, R. Q. Snurr, *Chem. Commun.* **2014**, *50*, 11329 – 11331.

[17] D. Yang, V. Bernales, T. Islamoglu, O. K. Farha, J. T. Hupp, C. J. Cramer, L. Gagliardi, B. C. Gates, *J. Am. Chem. Soc.* **2016**, *138*, 15189 – 15196.

[18] L. Grajciar, C. J. Heard, A. A. Bondarenko, M. V. Polynski, J. Meeprasert, E. A. Pidko, P. Nachtigall, *Chem. Soc. Rev.* **2018**, *47*, 8307 – 8348.

[19] a) S. M. J. Rogge, A. Bavykina, J. Hajek, H. Garcia, A. I. Olivos-Suarez, A. Sepulveda-Escribano, A. Vimont, G. Clet, P. Bazin, F. Kapteijn, M. Daturi, E. V. Ramos-Fernandez, F. X. Llabres i Xamena, V. Van Speybroeck, J. Gascon, *Chem. Soc. Rev.* **2017**, *46*, 3134 – 3184; b) P. Valvekens, F. Vermoortele, D. De Vos, *Catal. Sci. Technol.* **2013**, *3*, 1435 – 1445; c) J. Canivet, M. Vandichel, D. Farrusseng, *Dalton Trans.* **2016**, *45*, 4090 – 4099.

[20] a) J. Hajek, B. Bueken, M. Waroquier, D. De Vos, V. Van Speybroeck, *ChemCatChem* **2017**, *9*, 2203 – 2210; b) C. Caratelli, J. Hajek, F. G. Cirujano, M. Waroquier, F. X. L. I. Xamena, V. Van Speybroeck, *J. Catal.* **2017**, *352*, 401 – 414.

[21] F.-X. Coudert, R. Vuilleumier, A. Boutin, *ChemPhysChem* **2006**, *7*, 2464 – 2467.
[22] a) G. Kresse, J. Furthmuller, *Phys. Rev. B* **1996**, *54*, 11169 – 11186; b) G. Kresse, J. Furthmuller, *Comput. Mater. Sci.* **1996**, *6*, 15 – 50; c) G. Kresse, J. Hafner, *Phys. Rev. B Condens. Matter* **1993**, *47*, 558 – 561; d) G. Kresse, J. Hafner, *Phys. Rev. B Condens. Matter* **1994**, *49*, 14251 – 14269; e) G. Kresse, D. Joubert, *Phys. Rev. B* **1999**, *59*, 1758 – 1775.
[23] J. VandeVondele, M. Krack, F. Mohamed, M. Parrinello, T. Chassaing, J. Hutter, *Comput. Phys. Commun.* **2005**, *167*, 103 – 128.
[24] I. V. Alabugin, M. Manoharan, S. Peabody, F. Weinhold, *J. Am. Chem. Soc.* **2003**, *125*, 5973 – 5987.
[25] a) A. C. Fogarty, F.-X. Coudert, A. Boutin, D. Laage, *ChemPhysChem* **2014**, *15*, 521 – 529; b) G. R. Medders, F. Paesani, *J. Phys. Chem. Lett.* **2014**, *5*, 2897 – 2902.
[26] a) S. Dalla Bernardina, E. Paineau, J.-B. Brubach, P. Judeinstein, S. Rouzière, P. Launois, P. Roy, *J. Am. Chem. Soc.* **2016**, *138*, 10437 – 10443; b) G. Cicero, J. C. Grossman, E. Schwegler, F. Gygi, G. Galli, *J. Am. Chem. Soc.* **2008**, *130*, 1871 – 1878.
[27] J. Hajek, M. Vandichel, B. Van de Voorde, B. Bueken, D. De Vos, M. Waroquier, V. Van Speybroeck, *J. Catal.* **2015**, *331*, 1 – 12.
[28] a) A. Laio, F. L. Gervasio, *Rep. Prog. Phys.* **2008**, *71*, 126601; b) A. Laio, M. Parrinello, *Proc. Natl. Acad. Sci. USA* **2002**, *99*, 12562 – 12566; c) L. Maragliano, E. Vanden-Eijnden, *Chem. Phys. Lett.* **2006**, *426*, 168 – 175; d) Y. Sugita, Y. Okamoto, *Chem. Phys. Lett.* **1999**, *314*, 141 – 151; e) R. W. Zwanzig, *J. Chem. Phys.* **1954**, *22*, 1420 – 1426; f) V. Haigis, F.-X. Coudert, R. Vuilleumier, A. Boutin, A. H. Fuchs, *J. Phys. Chem. Lett.* **2015**, *6*, 4365 – 4370.
[29] J. K.-C. Lau, B. Ensing, *Phys. Chem. Chem. Phys.* **2010**, *12*, 10348 – 10355.
[30] G. Zahn, P. Zerner, J. Lippke, F. L. Kempf, S. Lilienthal, C. A. Schröder, A. M. Schneider, P. Behrens, *CrystEngComm* **2014**, *16*, 9198 – 9207.
[31] M. Kim, J. F. Cahill, Y. Su, K. A. Prather, S. M. Cohen, *Chem. Sci.* **2012**, *3*, 126 – 130.
[32] J. J. Low, A. I. Benin, P. Jakubczak, J. F. Abrahamian, S. A. Faheem, R. R. Willis, *J. Am. Chem. Soc.* **2009**, *131*, 15834 – 15842.
[33] R. E. Morris, L. Brammer, *Chem. Soc. Rev.* **2017**, *46*, 5444 – 5462.
[34] a) J. Canivet, A. Fateeva, Y. M. Guo, B. Coasne, D. Farrusseng, *Chem. Soc. Rev.* **2014**, *43*, 5594 – 5617; b) C. Wang, X. Liu, N. Keser Demir, J. P. Chen, K. Li, *Chem. Soc. Rev.* **2016**, *45*, 5107 – 5134.
[35] a) A. De Vos, K. Hendrickx, P. Van Der Voort, V. Van Speybroeck, K. Lejaeghere, *Chem. Mater.* **2017**, *29*, 3006 – 3019; b) S. M. J. Rogge, J. Wieme, L. Vanduyfhuys, S. Vandenbrande, G. Maurin, T. Verstraelen, M. Waroquier, V. Van Speybroeck, *Chem. Mater.* **2016**, *28*, 5721 – 5732.
[36] F. Formalik, M. Fischer, J. Rogacka, L. Firlej, B. Kuchta, *J. Chem. Phys.* **2018**, *149*, 064110.
[37] a) S. L. Ling, B. Slater, *Chem. Sci.* **2016**, *7*, 4706 – 4712; b) L. N. McHugh, M. J. McPherson, L. J. McCormick, S. A. Morris, P. S. Wheatley, S. J. Teat, D. McKay, D. M. Dawson, C. E. Sansome, S. E. Ashbrook, *Nat. Chem.* **2018**, *10*, 1096.
[38] I.-C. Lin, A. P. Seitsonen, I. Tavernelli, U. Rothlisberger, *J. Chem. Theory Comput.* **2012**, *8*, 3902 – 3910.
[39] P. E. Blöchl, *Phys. Rev. B* **1994**, *50*, 17953 – 17979.
[40] a) J. P. Perdew, K. Burke, M. Ernzerhof, *Phys. Rev. Lett.* **1996**, *77*, 3865 – 3868; b) J. P. Perdew, K. Burke, M. Ernzerhof, *Phys. Rev. Lett.* **1997**, *78*, 1396; c) S. Grimme, *J. Comput. Chem.* **2004**, *25*, 1463 – 1473; d) S. Grimme, J. Antony, S. Ehrlich, H. Krieg, *J. Chem. Phys.* **2010**, *132*, 154104.
[41] D. Dubbeldam, S. Calero, D. E. Ellis, R. Q. Snurr, *Mol. Simul.* **2016**, *42*, 81 – 101.
[42] G. A. Tribello, M. Bonomi, D. Branduardi, C. Camilloni, G. Bussi, *Comput. Phys. Commun.* **2014**, *185*, 604 – 613.
[43] S. Goedecker, M. Teter, J. Hutter, *Phys. Rev. B Condens. Matter* **1996**, *54*, 1703 – 1710.
[44] a) G. Lippert, J. Hutter, M. Parrinello, *Mol. Phys.* **1997**, *92*, 477 – 487; b) G. Lippert, J. Hutter, M. Parrinello, *Theor. Chem. Acc.* **1999**, *103*, 124 – 140.
[45] D. Frenkel, B. Smit, Academic Press, **2001**.
[46] G. J. Martyna, D. J. Tobias, M. L. Klein, *J. Chem. Phys.* **1994**, *101*, 4177 – 4189.

Manuscript received: July 11, 2019
Accepted manuscript online: August 28, 2019
Version of record online: October 31, 2019

